



ASME Accepted Manuscript Repository

Institutional Repository Cover Sheet

Cranfield Collection of E-Research - CERES

Fan flow field in an installed variable pitch fan operating in reverse thrust for a range of aircraft landing
ASME Paper Title: speeds

Authors: Rajendran DJ, Pachidis V

ASME Journal Title: Journal of Engineering for Gas Turbines and Power

Volume/Issue 141, Issue 10

Date of Publication (VOR* Online) 20.12.2019

ASME Digital Collection URL: <https://asmedigitalcollection.asme.org/gasturbinespower/article/doi/10.1115/1.4044686/975412/Fan-Flow-Field-in-an-Installed-Variable-Pitch-Fan>

DOI: [10.1115/1.4044686](https://doi.org/10.1115/1.4044686)

*VOR (version of record)

FAN FLOW FIELD IN AN INSTALLED VARIABLE PITCH FAN OPERATING IN REVERSE THRUST FOR A RANGE OF AIRCRAFT LANDING SPEEDS

David John Rajendran

Rolls Royce UTC, Cranfield University

Cranfield, Bedfordshire, United Kingdom

d.rajendran@cranfield.ac.uk

Vassilios Pachidis

Rolls Royce UTC, Cranfield University

Cranfield, Bedfordshire, United Kingdom

v.pachidis@cranfield.ac.uk

ABSTRACT

The installed flow field for a Variable Pitch Fan (VPF) operating in reverse thrust for the complete aircraft landing run is described in this paper. To do this, a VPF design to generate reverse thrust by reversing airflow direction is developed for a representative 40000 lbf modern high bypass ratio engine. Thereafter, to represent the actual flow conditions that the VPF would face, an engine model that includes the nacelle, core inlet splitter, outlet guide vanes, bypass nozzle, core exhaust duct, aft-body plug and core nozzle is designed. The engine model with the VPF is attached to a representative airframe in landing configuration to include the effects of installation. A rolling ground plane that mimics the runway during the landing run is also included to complete the model definition. 3D RANS solutions are carried out for two different VPF stagger angle settings and rotational speeds to obtain the fan flow field.

The dynamic installed VPF flow field is characterized by the interaction of the free stream and the reverse stream flows. The two streams meet in a shear layer in the fan passages and get deflected radially outwards before turning back onto themselves. The flow field changes with stagger setting, fan rotational speed and the aircraft landing speed because of the consequent changes in the momentum of the two streams. The description of the installed VPF flow field as generated in this study is necessary to: a) qualify VPF designs that are typically designed by considering only the uninstalled static flow field b) choose the VPF operating setting for different stages of the aircraft landing run.

INTRODUCTION

In a VPF, the pitch setting or stagger angle of the fan blades can be varied by an actuator located in the fan bullet-nose. Such control over the pitch setting can be used to optimize off-design fan operation without the need for a variable area bypass nozzle. Research studies comparing the VPF and variable area nozzle for modern high bypass ratio engine architectures have noted that the VPF can reduce aircraft mission fuel burn in the range of 3 to 7% [1-4]. VPF provides more fine control than the variable area nozzle in optimizing fan operation that makes it a better contender for future intelligent engines [4]. The mechanical design of pitch change actuator mechanisms that are housed within the fan bullet-nose have been demonstrated to be possible [5]. The lower mission fuel burn, adaptability to intelligent engine configurations and possibility to mechanically design the system has resulted in research interest in VPF. Additionally, if the VPF is used to generate reverse thrust, the bulky nacelle based cascade thrust reverser unit can be removed, paving the way for introducing ‘slim-line’ nacelle designs that can significantly reduce installation drag and weight. The combination of ‘slim-line’ nacelle and VPF for reverse thrust without the variable area nozzle and cascade thrust reverser unit can improve the aircraft mission fuel burn in the range of 10 to 15% [6]. The manner in which VPF can be used to generate reverse thrust by changing the direction of airflow is described in Appendix A.

The use of VPF to generate reverse thrust has been studied by NASA in the Quiet Clean Short-haul Experimental Engine (QCSEE) and the Advanced Ducted Propulsor (ADP) programs. In the QCSEE program, two VPF designs were developed and characterized in reverse flow using an experimental test rig that included a clean flow path of only the VPF and guide vanes [7, 8]. From these designs, one was chosen and tested in an outdoor test rig with the VPF shrouded in a nacelle and a modified outlet nozzle featuring flared petals to aid flow in reverse thrust operation. These tests verified the feasibility of the design to establish a reverse flow stream at different fan rotational speeds [9, 10]. A few wind tunnel tests were also conducted in uninstalled conditions with the modified flared outlet nozzles to study the effect of crosswind and forward velocity. The wind-tunnel results were presented in terms of overall force parameters and no information on the general or fan flow field, even in the uninstalled tunnel conditions, could be obtained because of lack of instrumentation [11]. In the ADP program, a low noise low pressure ratio VPF design that is representative of modern high bypass ratio engines was developed. A 22 inch model of the ADP design was tested in a rig that included the nacelle, unmodified nozzle, guide vanes and core engine splitter [12, 13]. The rig results quantified the fan flow characteristics only in static conditions for different stagger angle settings. The flow field in the rig was analyzed computationally by using 3D RANS simulations and the uninstalled fan flow field was described

only in two nominal VPF operating conditions and not in reverse flow conditions [14]. Further in a recent study, the uninstalled flow field for the ADP in reverse flow regime at static conditions was computed using 3D RANS simulations [15].

Computational or rig studies have not been carried out to describe the installed VPF fan flow field in reverse flow for different aircraft landing speeds. However, such information is required to assess the feasibility of using VPF for reverse thrust to replace conventional cascade based thrust reversers. Therefore, in this study, the installed fan flow field of a VPF in a modern high bypass ratio engine is computationally obtained for a range of free stream velocities that is representative of actual operating conditions. The installed dynamic fan flow field is different from the reported uninstalled static flow field that is conventionally considered when designing and testing VPF configurations.

MODEL DEVELOPMENT

The objective of the study is to obtain the fan flow field in the VPF of a modern high bypass ratio engine operating in reverse thrust mode as installed in an aircraft during its landing run. To meet the objective four models were developed: 1. Engine model with flow path 2. VPF, Outlet Guide Vane (OGV) design to meet engine specifications 3. Airframe in landing configuration 4. Pylon and Nacelle for installing engine to the airframe.

Engine Model

The engine thermodynamic cycle for the representative 40000 lbf modern high bypass ratio engine is defined in TURBOMATCH, an in-house engine gas dynamic model [16]. The engine architecture is a two-spool geared configuration with 110 inch fan inlet diameter and a bypass ratio of 14 at design point. A multi-objective genetic algorithm optimizer with engine specific fuel consumption and weight as objective functions, and the mission requirements at different flight segments as constraints, was used to optimize the engine thermodynamic cycle [17]. The 1D engine hot and cold gas flow path is generated for the optimized cycle using ATLAS, an in-house mean-line and weight estimation code [18, 19]. In the present study to completely describe the installed fan flow field, it is considered sufficient to model the VPF flow path including the spinner, the splitter into the core engine, the bypass nozzle flow path with the OGV, and a portion of the core nozzle duct after the turbines with the aft-body plug as shown in Fig. 1. The spinner and splitter geometrical designs are scaled to the required engine dimensions from a design database. The lines of the bypass nozzle, core exhaust nozzle duct and aft-body plugs are obtained from the flow path definition tool.

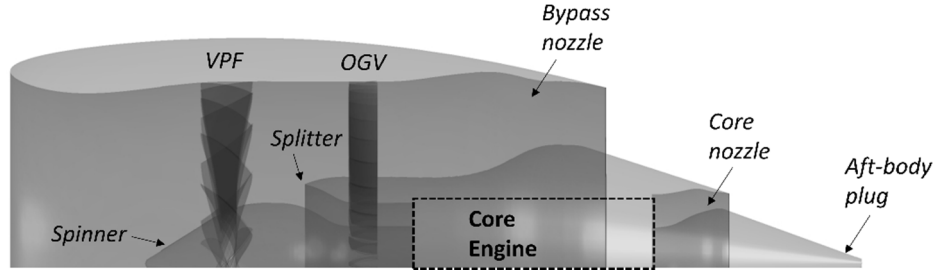


Fig. 1 Engine internal flow path representation in model

VPF and OGV

The VPF design is developed using the ADP design as baseline. The ADP design is chosen as the baseline because of it being a modern high bypass ratio engine design that has been extensively validated and tested [13]. The ADP design is scaled from the original 22 inch to 110 inch fan diameter of the engine model. The ADP design has a hub-to-tip radius ratio (r_h/r_t) of 0.42. This value is not suitable for the present engine model because it would lead to an unacceptably high value of fan flow coefficient and consequently to significant losses in performance. Therefore, r_h/r_t of the scaled model is modified to a value of 0.3 to keep the flow coefficient in the acceptable range. A through-flow analysis of the 0.3 r_h/r_t fan is carried out using, SOCRATES, an in-house streamline curvature based through-flow code [20]. Based on the analysis, the stagger and flow angles of different span-wise airfoil profiles are modified to get the same non-dimensional work distribution as the baseline design. The analysis indicated that the profiles up to 10% of the span from the hub are choked at the nominal design point. Therefore, the location of maximum thickness and stagger angle of the airfoil profiles in the hub region are modified to relieve the choking. The updated VPF design is then numerically characterized in forward flow and the results are validated using experimentally generated characteristics of the ADP test program. A comparison of the baseline ADP fan and the VPF design for the present study is shown in Table 1.

The stagger angle of the VPF design is rotated by 90° through feather pitch from the nominal forward flow setting to establish the reverse stream. The behavior of the VPF design in reverse thrust is characterized at two fan rotational speeds: N_1 and $N_2 = 0.8N_1$, and three stagger angle settings: ζ_1° , $\zeta_2^\circ = \zeta_1^\circ - 6^\circ$, and $\zeta_3^\circ = \zeta_1^\circ - 12^\circ$. The values of the stagger angles are within $\pm 10^\circ$ from the rotated 90° position. The reverse flow characteristics are generated using 3D RANS by using a computational domain that includes only the VPF. The objective of the VPF only characterization is to verify the reverse flow handling ability of the design and to choose stagger angle settings to be explored further in the installed configuration. The non-dimensional characteristics of the VPF in reverse flow are shown in Fig. 2. The

OGV for the present study is scaled from the ADP OGV. The inlet angles of the scaled OGV are corrected to match the flow angles from the VPF.

Table 1 – Comparison of ADP and VPF designs

Parameter	Baseline ADP	VPF Design
Outer diameter (in)	22	110
Pressure Ratio	1.28	1.27
Temperature Ratio	1.08	1.08
RPM	8400	1680
Tip speed (m/s)	245	245
Hub to tip ratio	0.42	0.3

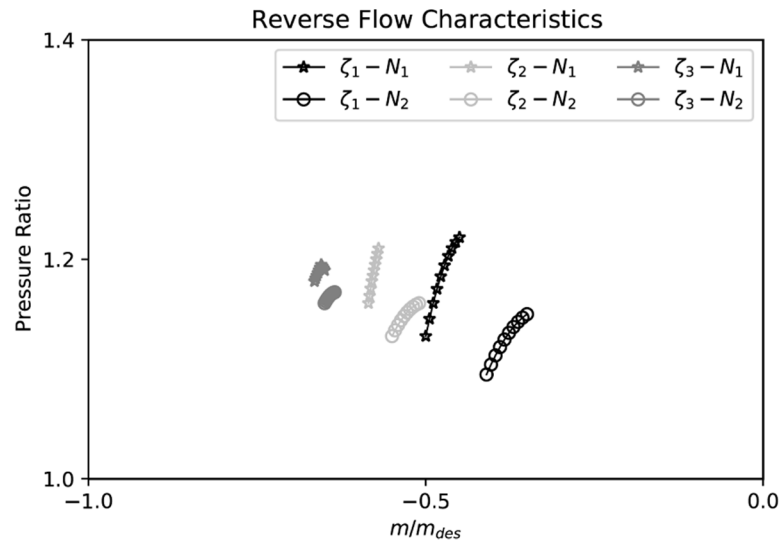


Fig. 2 VPF reverse flow characteristics for three setting angles and rotational speeds

Airframe in Landing Configuration

The DLR F11 airframe is used as the baseline in the present study. DLR F11 is a derivative of NASA Common Research Model (CRM) with wing flaps and slats in fully deployed configuration that is representative of the landing aircraft [21, 22]. The baseline airframe is scaled to dimensions that are typical for an airframe that uses two 40000 lbf turbofans. The flow over the scaled airframe is validated by comparing numerical 3D RANS results with experimental

pressure distributions and non-dimensional force coefficients. Inboard and outboard spoilers with spoiler-wing ratio of 4.1 are added to the scaled airframe at a typical 50° deployment angle. The design of the spoiler is validated by comparing the increase in drag-coefficient with similar designs [23]. A rolling ground plane is added with a typical engine ground clearance to mimic the run-way during the landing run.

Nacelle and Pylon

The engine is wrapped in a short cowl axisymmetric nacelle generated using GEMINI, an in-house nacelle design tool [24]. The tool parametrizes the nacelle design into 10 geometric variables and modifies the nacelle aerodynamic lines to obtain minimum drag coefficient. The engine wrapped in the nacelle is attached to the airframe wing using a pylon. The location of the engine with reference to the airframe is fixed based on an engine installation aerodynamics study to minimize the installation drag [25]. The ground clearance after the engine is installed in the airframe is 0.6 m. The pylon construction is based on symmetric NACA profiles, the chord length and thickness of which are determined from relative engine location and structural integrity requirements. The pylon strut located in the bypass nozzle results in a reduction of the nozzle exit flow area. The bypass nozzle flow path contours are modified to match the bypass exit area required from the engine thermodynamic model.

Installed Research Model

The installed research model is defined by attaching the engine wrapped in a nacelle to the airframe through the pylon. The engine internal flow path has full annular 360° representations of the bypass nozzle with the pylon strut, 40 OGV airfoils, splitter duct and 18 fan blades to capture 3D non-axisymmetric flow features. A symmetric half of the installed research model is placed in a cuboidal far-field domain that is approximately two airframe fuselage lengths in longitudinal, lateral and vertical directions with the base bound by the ground plane as shown in Fig. 3.

COMPUTATIONAL DOMAIN DISCRETIZATION

A hybrid domain discretization strategy is followed for grid generation of the installed research model. The domain discretization is done by dividing the computational domain into two regions: 1. External to the engine and 2. Internal engine flow path components.

External Region

The external region consists of: a) airframe b) nacelle contour covering the engine c) external portion of the pylon d) the wing with flap, slats and spoilers deployed e) far-field f) ground plane. When the VPF operates in reverse thrust,

the engine sucks in mass flow through the bypass nozzle exit from the external region. Therefore, the external region flow field solution imposes the boundary conditions for the engine internal flow-path components. Unstructured grids using the robust Octree method are generated for the external region with finely resolved near wall elements with y^+ less than one on the wing, spoiler, pylon and nacelle surfaces. The growth ratio of the unstructured elements are specified as a linear function away from the surfaces to avoid unnecessary resolution of far-field flow that will lead to large grid sizes, while restricting the element aspect ratio to be less than 100 in the entire region. Specially defined grid refinement density boxes are used in the nacelle-fan interface and the bypass nozzle exit interface to populate grid elements in the external volumetric regions that transfer the flow boundary conditions into the engine. The unstructured domain quality index that measures the scaled element aspect ratio is in the acceptable range of 0.4 to 0.6, where 1 indicates a perfectly regular element and 0 a null volume element. The size of the grid is finalized using a Grid Convergence Index (GCI) study of the resultant force on the wetted surfaces obtained from wall shear and pressure distributions as parameters. The finalized grid has ~30 million elements in the asymptotic parameter value region with a maximum GCI of 0.006 obtained from Richardson extrapolation method.

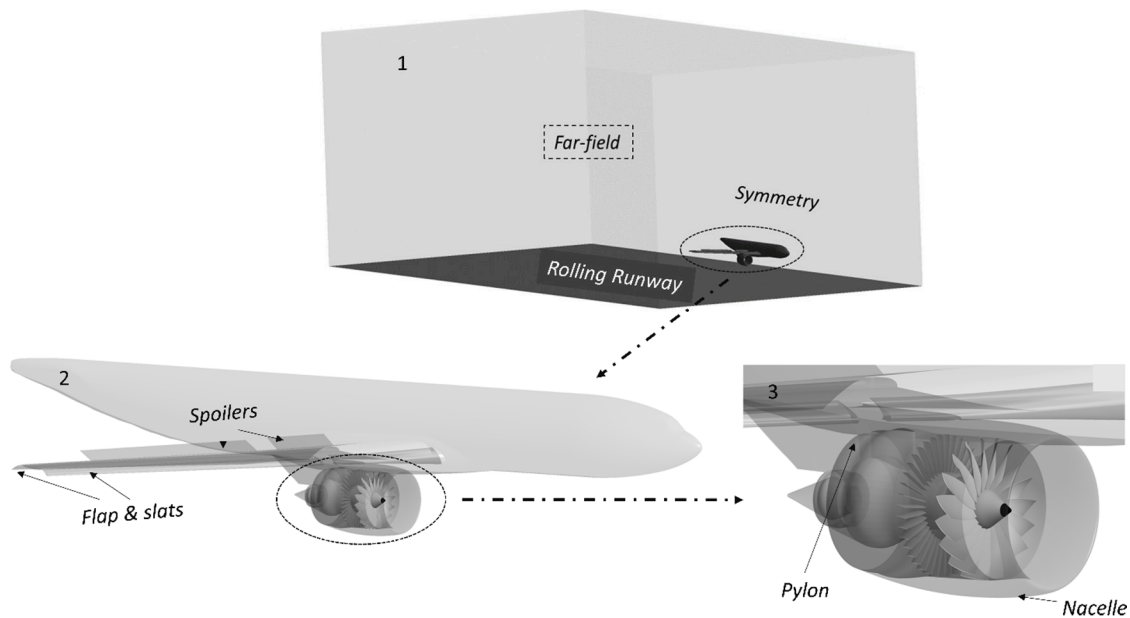


Fig. 3 Schematic showing development of installed research model

Internal Region

The internal region consists of two types of components: a) Duct components – Bypass nozzle with pylon strut, core engine splitter and core nozzle b) Turbomachinery components – VPF and OGV. In the duct components, the

bypass nozzle with the pylon strut is discretized using unstructured elements with wall y^+ less than 1. Unstructured grid is chosen for the bypass nozzle because the flow direction is not known a priori at the external interface to align the structured grid. For the splitter and core nozzle, a structured grid with flow aligned elements is used. O-grid with y^+ less than 1 is used to capture the near wall flow physics. A quarter O-grid topology is adopted at the sharp splitter edge to ensure smooth flow of grid elements around the corner. The skew angle of the structured grid elements of the duct components are in the acceptable range of 45° to 135° with aspect ratios less than 100 and a near wall expansion ratio less than 1.2.

Multi-block structured discretization strategy is followed for the turbomachinery components. An H-J grid topology with O grid blocks near the walls is used for the VPF because of the high reverse flow stagger angle. A simple H-O grid topology is sufficient for the low stagger OGV airfoils. The leading edge and trailing edges are resolved using rounded flow aligned O-grid elements. The skew angle of the VPF and OGV grids are in the acceptable range of 30° to 150° , with aspect ratios less than 80 and near wall expansion ratios less than 1.1. Extensive GCI study is carried out to optimize the grid size and to quantify numerical uncertainty. The parameters considered are the span-wise distributions of Mach numbers and flow angles across different stations and global parameters like mass flow and pressure ratio. A gross GCI value, defined as the RMS of the averaged span-wise parameters and the global parameters, is used to compare the different grids. The finalized internal grid has ~ 43 million elements and a gross GCI of 0.004 obtained from Richardson extrapolation. The grid size is higher than the external region because of the full annular flow path representation. The surface grid on portions of the external region and the internal region is shown in Fig. 4.

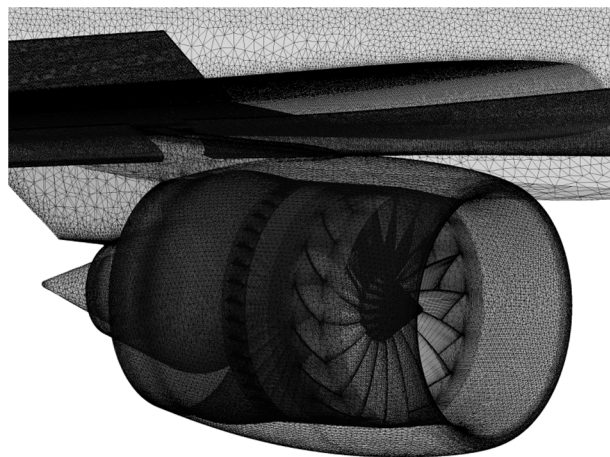


Fig. 4 Representative grids on portions of external region and engine internal flow-path

SOLUTION MATRIX

From a study of the clean VPF only reverse flow characteristics shown in Fig. 2, it is decided to explore the installed flow field for two stagger angle settings, ζ_1° and ζ_2° . The stagger angles are chosen because of the wide operating range of the speed lines. Two sets of VPF grids are generated to represent the change in the fan geometry because of the change in the stagger setting angle. For each stagger angle setting of the VPF, the solution is obtained for two fan rotational speeds, N_1 and N_2 , to capture the bounds of behavior in the clean reverse flow characteristics. Each stagger angle-rotational speed combination is solved for a range of aircraft landing speeds from 140 to 20 knots in steps of 10 knots. Therefore, the two sets of integrated models, at each stagger angle setting that is run for two different fan speeds for the landing run, results in a total of 60 solutions as shown in Table 2.

Table 2 – Matrix of solutions

Fan Stagger	Fan RPM	Landing Speed
degrees	%	knots
ζ_1	N_1	140 to 20 in steps of 10
ζ_1	N_2	
ζ_2	N_1	
ζ_2	N_2	

BOUNDARY CONDITIONS AND SOLUTION

The 3D RANS solution of the flow field is obtained using ANSYS-CFX, a coupled finite volume solver that uses element based interpolation shape functions. The RANS equations are solved in a fully implicit manner with second order resolution of conservation and turbulence equations to minimize discretization errors. The effects of turbulence are modelled using the two-equation $k-\omega$ Shear Stress Transport (SST) model. The near-wall flow physics is resolved without the requirement of imposing wall-functions because of explicit grid refinement at all wall surfaces that are specified as adiabatic no slip walls.

The boundary conditions that are specified to obtain the flow field solution are: 1. Fluid velocity at far field inlet 2. Fan rotational speed 3. Steady state thermodynamic parameters that represent the core engine: Axial velocity and

total temperature at core engine inlet after the splitter edge and core engine exhaust duct outlet 4. Far-field conditions specified at ambient atmospheric pressure and temperature with flow entrainment and zero gradient of turbulence parameters 5. Ground plane moving at the same velocity as the far field fluid velocity. The core engine thermodynamic parameters are obtained from the engine performance model to sustain fan operation at the specific rotational speed and stagger angle combination. The transition plane into the internal flow path at the fan inlet and the fan outlet-splitter inlet junction are specified as frozen rotor interfaces because of the change in frames of reference between stationary and rotating domains. The transition planes at the bypass and core nozzle exits into the external region, OGV outlet-bypass nozzle inlet junction and splitter-OGV inlet are specified as fluid-fluid interfaces. The combination of the boundary conditions and the interfaces complete a well-posed problem definition for the present model to obtain numerical solution of the RANS equations. A schematic representation showing the boundary conditions and interface definitions are shown in Fig. 5.

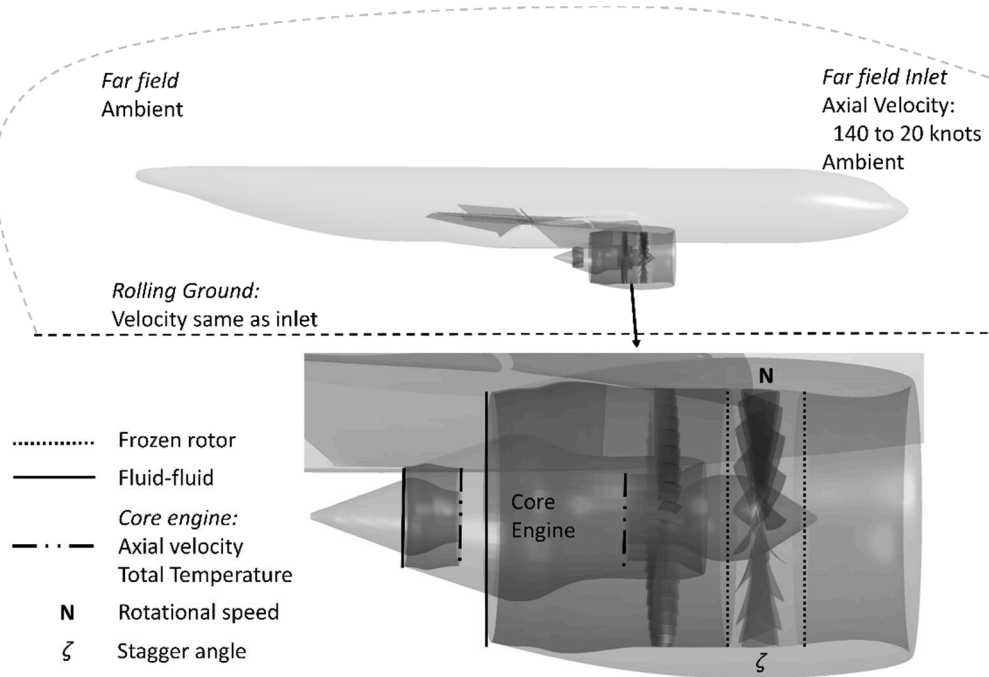


Fig. 5 Schematic representation of boundary conditions and interface definition

Three different physical advection timescales for the flow to traverse the domains once are identified in different parts of the computational domain: 5s in the far-field domain, 0.04s in the engine internal flow path and 0.003s in the rotating VPF domain. Therefore adaptive time-scale factors are used in different parts of the domain to properly resolve the flow physics and to improve the rate of convergence. The solution is considered to be converged when the

RMS value of the standard deviation over 50 iteration steps of global and local parameters of interest such as the net force, fluxes and Mach numbers, are within 0.5% of the mean of standard deviations over 25 iteration steps and the current iteration value. This convergence strategy is adopted to ensure proper resolution of changes in the parameters arising because of local zones of recirculation. The solution is carried out in a High Performance Computing (HPC) facility ‘DELTA’ at Cranfield using a Platform Message Passing Interface (MPI) based parallelization scheme. DELTA has a peak processing speed of 60 Teraflops, and a total of 1888 cores with a shared memory of 15 TB. Typically, 4 chunks of 16 CPUs each with 16 parallel MPI processes are used for the analyses. The run time for a single simulation with simultaneous statistical processing of the data to determine convergence is around 24 hours.

RESULTS AND DISCUSSIONS

To completely describe the installed fan flow field of the VPF in reverse thrust at different landing speeds, the results are presented in the following sequence:

1. The installed configuration differs from the uninstalled configuration in terms of the flow conditions that the VPF will need to operate. Therefore, initially a description of the installed general flow field in the integrated airframe-engine model at a landing speed of 110 knots is provided.
2. The fan flow field in the ζ_1° stagger and N_1 fan rotational speed setting, at 110 knots is described.
3. The change in the fan flow field with change in stagger from ζ_1° to ζ_2° at the same N_1 fan rotational speed and landing speed of 110 knots is described.
4. The change in the fan flow field with change in fan rotational speed from N_1 to N_2 at ζ_1° stagger and landing speed of 110 knots is described.
5. The change in the fan flow field with change in the landing speed of the aircraft is described by considering the VPF at ζ_1° stagger and N_1 fan rotational speed.

Installed General Flow Field

The general flow field around the airframe and within the engine for the VPF at ζ_1° stagger and N_1 fan rotational speed at 110 knots landing speed is described here. When the VPF is operating in reverse thrust mode, the flow is injected from the bypass nozzle exit and ejected from the fan inlet. The general flow field can be described by considering the external flow and internal flow in the engine.

External Flow Field

The flow streamlines external to the engine are shown in Fig. 6.

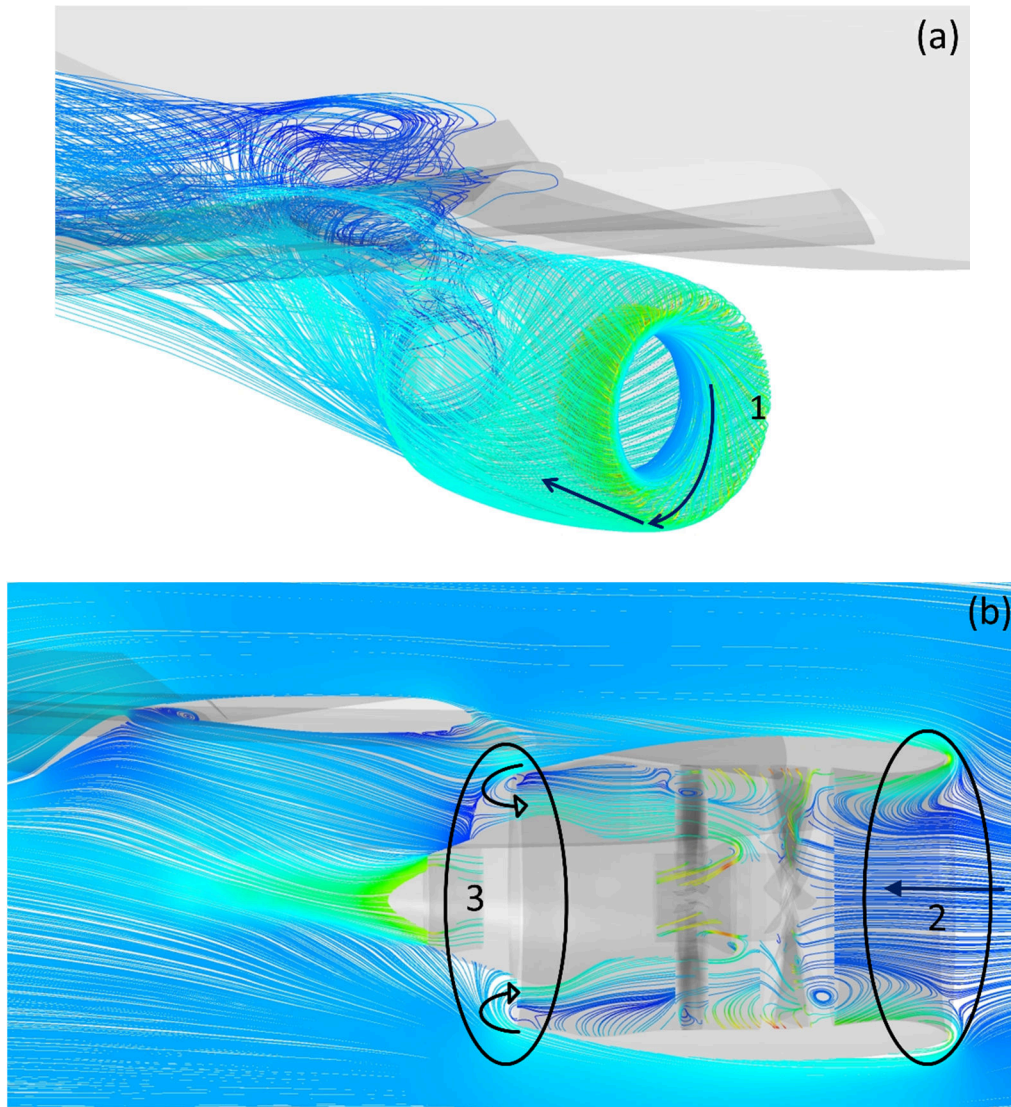


Fig. 6 External flow – (a) 3D streamlines emanating from fan inlet plane to the external far-field domain (b)

Streamlines on a 2D plane defined at mid-engine location into airframe

There are three major flow features marked in Fig. 6:

1 – The flow that exits the fan inlet plane comes swirling out at an angle. This flow when it reaches the nacelle lip is washed down by the free stream flow. The flow continues swirling down the nacelle till it reaches the bypass nozzle exit plane where it comes under the influence of fan suction.

2 – The free stream flow penetrates into the nacelle and the reverse flow stream exists only in the radially outer annular regions of the nacelle. A part of the penetrating free stream flow is entrained by the reverse flow and is added

to the stream that is coming out into the nacelle lip. The swirl angle of the flow out towards the nacelle lip is fixed by the interaction of the reverse stream out of the fan inlet and the entrained free stream flow. The swirl angle of the flow that is washed down the nacelle lip towards the bypass nozzle exit is fixed by the interaction between the external free stream flow and the reverse stream flow. The remaining portion of the free stream flow that is not entrained enters the fan passages at the inlet in the conventional forward flow direction.

3 – The fan suction is felt at the bypass nozzle exit plane. This causes a part of the flow over the nacelle to turn 180° into the bypass nozzle exit to set up the reverse stream. The effect of fan suction sets up a shear layer near the engine exit region that divides the flow into that which turns back into the engine and that which escapes the suction. The flow that does not turn into the engine in the free stream is deflected towards the wing because of the effect of suction and the deployed wing pressure field. This can be observed clearly in the flow streamlines near the ground plane.

The flow-field external to the engine has circumferential variations around the engine annulus. Fig. 7 shows vector plots at three planes, marked 1, 2 and 3, along the length of the aircraft. In the plane 1, the bottom portion of the reverse flow is influenced by the ground plane. The ground plane causes a circumferential variation in the free stream flow that spreads around the engine. The ground plane and the nacelle bottom surface squeezes the free stream and reverse stream flow at the bottom surface that causes a circumferentially varying flow field around the nacelle. This circumferential variation is then convected downstream that leads to differences in the swirl velocity around the annulus as can be seen in Plane 2. The swirling flow of varying strength along the circumference induces vorticity in the free stream flow in the immediate vicinity of the nacelle that further accentuates the circumferential variation of the external flow field. As the flow reaches Plane 3, it encounters the pylon that presents a physical separation between the flows in the inboard and outboard sides of the wing. The flow swirl is such that there is an accumulation of flow on the outboard pylon side of the wing. It is on such a flow field at the engine exit that has significant circumferential variations that the fan suction acts. This causes the location of the flow turn shear layer with reference to the bypass nozzle exit plane to vary around the annulus. This can be seen in the flow feature marked 3 in Fig.6 (b), where a larger amount of mass flow is entering the bottom portion of the engine compared to the top part because of flow migration and accumulation toward the outboard side of the wing.

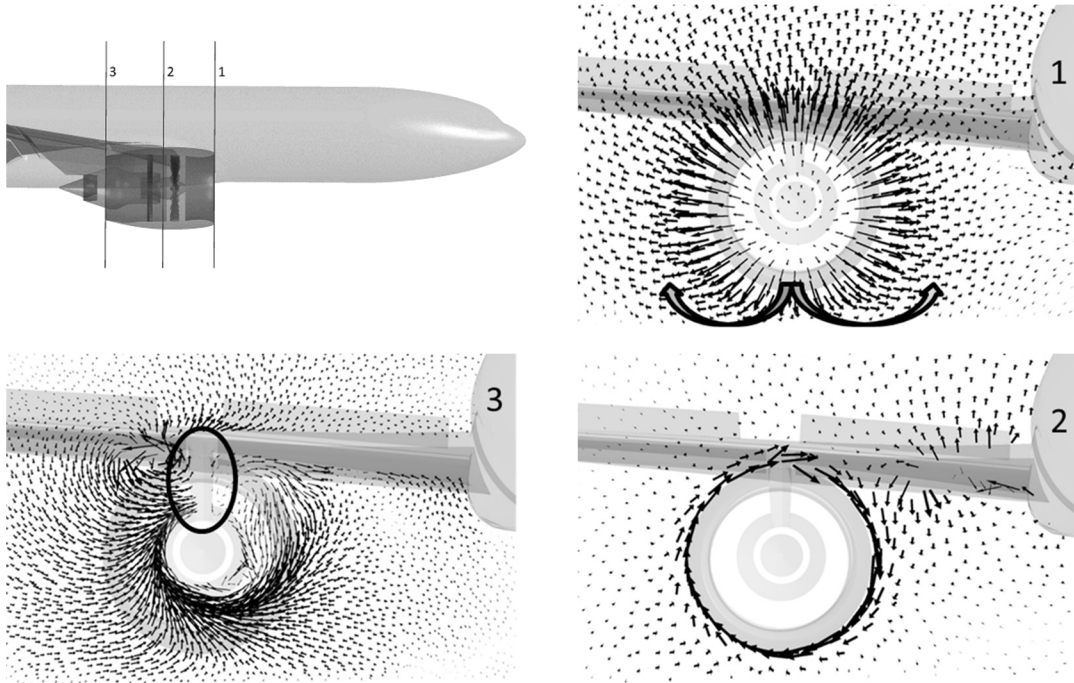


Fig. 7 External flow – Vector plots on planes along the length of the aircraft showing circumferential variation

Internal Flow Field

The flow streamlines within the engine are shown in Fig. 8.

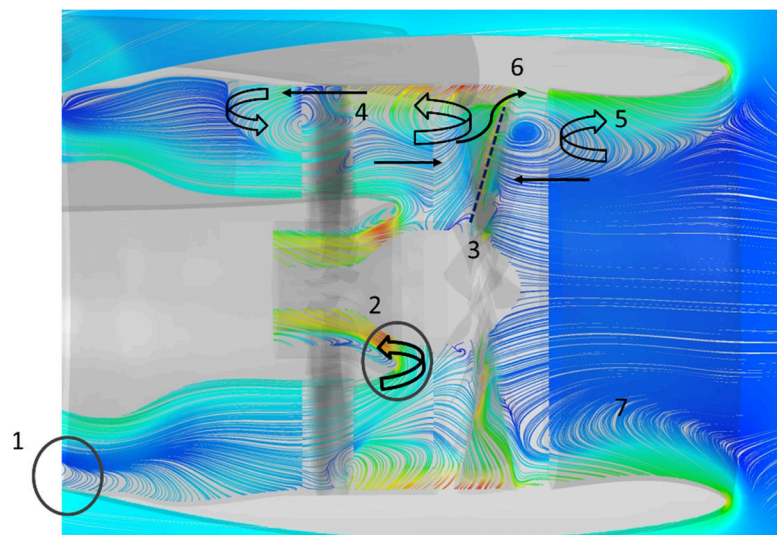


Fig. 8 Internal flow – Streamlines on a 2D plane defined at mid-engine location showing major flow features

The reverse flow within the engine has seven major features as marked in Fig. 8:

1 – The 180° turn into the engine from the external flow field causes a recirculation zone at the bypass nozzle lip.

2 – The reverse flow develops through the bypass nozzle duct and the OGV. As it reaches the splitter edge, one portion of the flow turns another 180° to feed the core engine. This turn results in separated flow at the sharp splitter edge. The amount of flow entering the core engine depends on the core engine operating point on the working line to sustain the fan rotational speed.

3 – The remaining portion of the reverse flow enters into the fan passages at the outlet. Within the fan, the reverse flow meets the free stream flow in a shear layer marked by dotted lines.

4 & 5 – Both the reverse stream and free stream flow are deflected radially outwards and are turned back on to themselves. The flow feature marked 4 is turned back towards the bypass nozzle through the radially outer span portions of the OGV. This flow eventually meets the reverse stream from the bypass exit and is rolled back to rejoin the reverse stream. In the flow feature marked 5, the free stream is turned back towards the nacelle inlet and joins the reverse stream that proceeds down to nacelle lip.

6 – A portion of the reverse stream escapes near the radially outer spans of the fan at the inlet plane to set up the reverse stream. It is this reverse stream that entrains the free stream flow and flows out towards the nacelle lip.

7 – This feature is marked to represent the circumferentially varying nature of the flow through the engine as can be observed from the differences between the top and bottom portions of the streamlines shown in Fig. 8. This difference is a consequence of the flow field external to the engine from which the reverse stream is established. The extent of circumferential variation across different stream-wise planes through the engine can be observed from the Mach number contours shown in Fig. 9. In the bypass duct, the circumferential variation of the recirculation zone ‘1’ can be observed in the slices marked, 1 and 2. The interaction of the pylon wake and the signature of the rolling flow ‘4’ can be observed from slices 3 and 4. The bi-directional flow in the OGV passages, with the radially outer span portion towards the bypass nozzle exit and the radially inner span portion towards the fan is apparent in the wake signature at the OGV-splitter interface. The signature of the flow entering at the fan inlet and outlet plane can be observed in the radially inward portion of the splitter-fan interface and the fan inlet plane. The reverse stream flow ‘6’ that escapes the fan passages can be identified by the wake signature at the radially outward portion of fan span near the annulus tip. The zone of transition between the free stream flow and reverse flow is observed as an entrainment ring zone in the fan inlet plane.

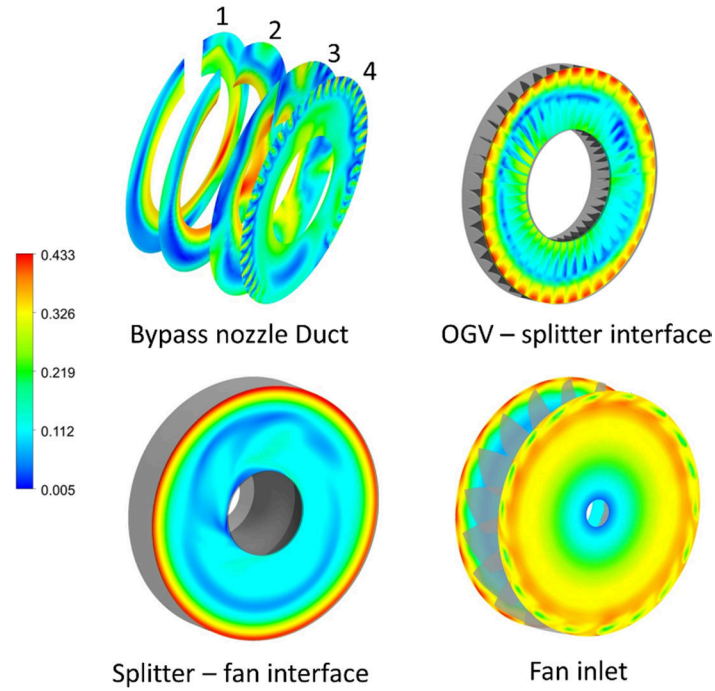


Fig. 9 Internal flow – Mach number contours at different stream-wise locations within the engine

The general flow field changes with the aircraft landing speed. The internal and external flow features marked at 110 knots are present at other landing speeds as well. As the landing speed reduces, the momentum of the free stream reduces, which reduces the extent of penetration of free stream into the nacelle. The mass flow of reverse stream sucked in at the bypass nozzle exit increases because of the presence of larger amount of slower free stream which can be captured by the fan suction at the exit. These changes lead to changes in the extent and strength of the flow features at 110 knots. Since the objective is to describe the fan flow field in the VPF, a detailed discussion of the change in the general flow field at other landing speeds is superfluous. However, the consequence of the change in the general flow field is the resulting change in the flow conditions at the fan inlet and outlet planes which are described in the following sections.

ζ_I° Stagger - N_I Speed VPF Fan Flow Field at 110 knots

The fan flow field is defined by the interaction of the reverse stream and the free stream. The circumferentially averaged meridional vector plot of the absolute velocity and the span-wise variation of axial velocity are shown in Fig. 10.

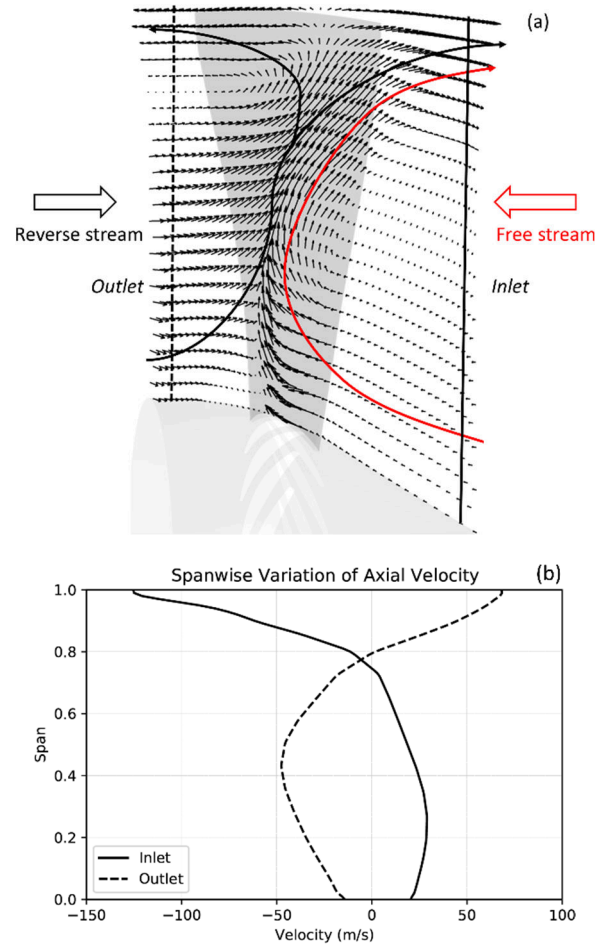


Fig. 10 Fan flow field – (a) Meridional velocity vectors showing reverse stream and free stream (b) Span-wise variation of circumferentially averaged axial velocity

It can be observed from the vector plot that the free stream and the reverse stream meet in the fan passages and are deflected radially outwards toward the fan casing. The deflected reverse stream branches into two streams: one escaping out at the fan inlet and another turning back out through the fan outlet plane. The free stream is turned back onto itself and joins the escaping reverse stream at the fan inlet. This results in a novel bi-directional flow at both the fan inlet and outlet planes that can be observed from the direction of the axial velocity in Fig. 10 (b). The nominal forward direction (inlet to outlet) is considered positive for the axial velocity. At the inlet plane: a) there is a reduction in the axial velocity from 20% to 75% of the span. This decrease is indicative of the free stream flow gradually turning onto itself. A small decrease is observed from 20% of the span to the hub because of boundary layer effects. b) After 75% span, the direction of the flow changes towards the nacelle inlet and the absolute axial velocity shows an increasing trend towards the casing. At the outlet plane: a) the axial velocity of the reverse stream peaks at nearly 40%

span and shows an decreasing trend till 80% span. This peaking is a consequence of a portion of the reverse stream turning into the core engine at the splitter edge before reaching the fan outlet plane. b) After 80% span, the direction changes towards the bypass nozzle and the absolute velocity increases till it reaches the casing.

The absolute magnitude of the reverse flow out into the nacelle at the inlet plane (75% span to casing) is nearly twice the amount of reverse stream turned back into the engine at the outlet plane (80% span to casing). This is because of two reasons: 1. the momentum of the reverse stream flux is higher, as can be noted from higher axial velocity of reverse stream at outlet. This causes the reverse stream to dominate as both the streams are deflected radially outwards and establish an outward flowing reverse flow towards the nacelle at the inlet plane. The flow turned back into the engine is the remaining portion that did not manage to escape out towards the nacelle 2. The reverse flow at the inlet also contains the free stream flow that is entrained and turned back on to itself to contribute further to the escaping reverse stream.

Even though the circumferentially averaged axial velocity is sufficient to describe the flow field in the VPF, circumferential variations exist in the axial velocity which can provide further insight into flow field. The circumferential variation in the axial velocity at the fan inlet and outlet plane is shown in Fig. 11. In the inlet plane: Wake signatures are noticeable only at 90% span. This is because only at this span the reverse stream escapes out into the fan inlet from within the fan blade passages. At 80% span, the reverse flow towards nacelle consists of the free stream that is turned back before entering the fan passages. The free stream flow in the forward direction before it is turned back is observed at 20% and 50% span. At the outlet plane: Wake signatures are noticeable in the 80% and 90% span because all the reverse stream that turns back does so from within the fan blade passages. The circumferential variations at 20% and 50% span are because of the development of the reverse flow through the bypass nozzle and the OGV passages.

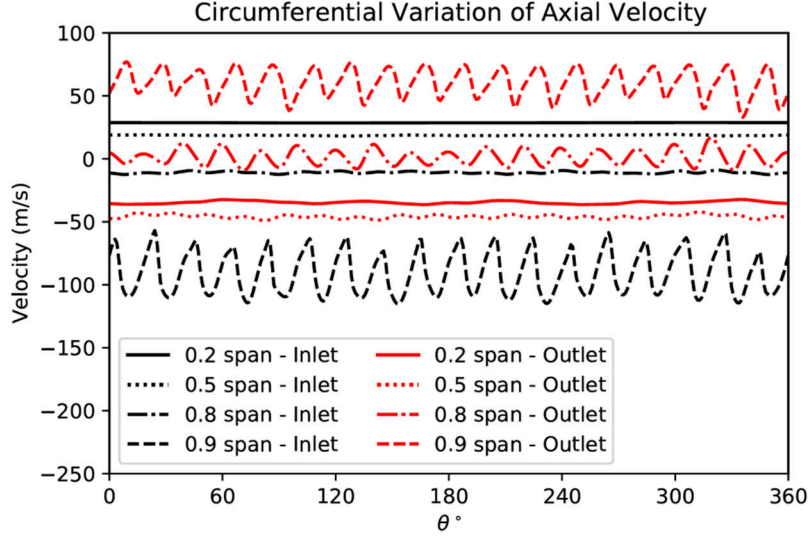


Fig. 11 Fan flow field – Circumferential variation of axial velocity at different span-wise locations

This installed VPF fan flow field with both free stream and reverse stream is different from that of an uninstalled clean reverse flow because of two reasons: 1. the absence of free stream 2. Even if free stream is included in an uninstalled analysis, the boundary flow conditions and modeling is not sufficient to resolve the bi-directional flow at the fan inlet and outlet planes. Therefore, this kind of explicit installed modeling is necessary to quantify the installed behavior of VPF in reverse thrust.

Effect of Stagger Setting on Fan Flow Field

The change in the fan flow field when the VPF stagger angle setting is changed from ζ_1° to ζ_2° at N_I fan rotational speed and 110 knots landing speed is described in this section. The passages of the stagger setting ζ_2° is 6° more open than ζ_1° . A comparison of span-wise variation of axial velocities for the different stagger angle settings are shown in Fig. 12.

The VPF only clean reverse flow characteristics, in Fig. 2, suggests that the reverse stream mass flow of the ζ_2° setting will be higher than the ζ_1° setting. However, this is not the case. In the installed condition with both the streams, since the passages are more open in the ζ_2° stagger setting, a higher amount of free stream flow penetrates into the fan passages. This can be observed in the higher magnitude of axial velocity at the inlet plane for the ζ_2° stagger setting from hub to 75% span. The consequence of this higher free stream penetration is that the reverse stream is not able to enter into the fan passages as much as in the ζ_1° stagger setting. This can be observed from the lower axial velocity of

the ζ_2° setting at the fan outlet plane from hub to 10% of span. Therefore, a larger amount of the reverse stream of the ζ_2° stagger setting is turned back on to itself as can be seen in the higher magnitude of velocity vectors near the casing (90% to 100%) at the fan outlet plane. Because a larger amount of the reverse stream is turned back, the reverse stream exiting near the fan inlet casing is lower than the ζ_1° stagger setting. This is different from the case in which only the reverse stream exists because in that case the more open passages of the ζ_2° stagger setting would have resulted in a higher amount of reverse flow at the fan inlet.

The significant change in the flow field because of installation and interaction of the free stream and reverse stream demonstrates how the VPF only clean reverse flow characteristics can be misleading when choosing the setting of VPF in an actual installed engine during the aircraft landing run.

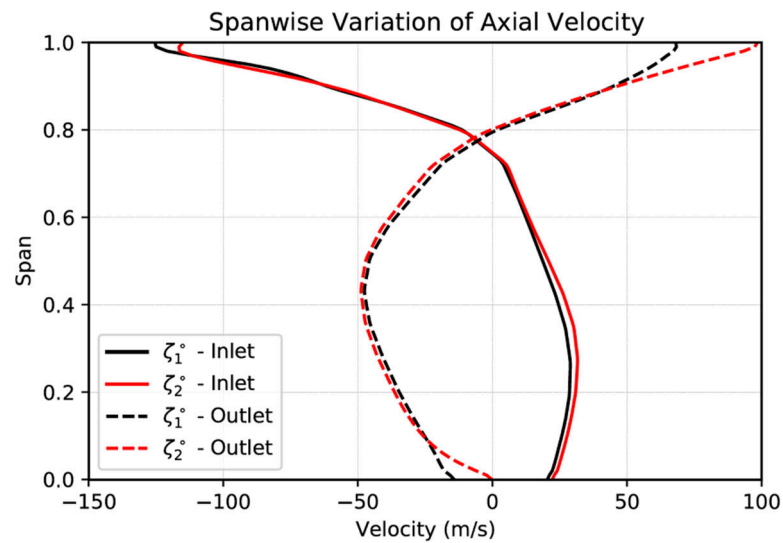


Fig. 12 Effect of stagger change - Span-wise averaged axial velocity plot

Effect of Rotational Speed on Fan Flow Field

The change in the fan flow field when the rotational speed is changed from N_1 to N_2 for the ζ_1° stagger setting at a landing speed of 110 knots is described in this section. The rotational speed, N_1 is 20% higher than N_2 . A comparison of the circumferentially averaged meridional absolute velocity vector plots and span-wise variation of axial velocities for different speeds are shown in Fig. 13. As the rotational speed is decreased, the effect of fan suction is weaker and a lower amount of mass flow with lower momentum is sucked from the bypass nozzle exit. This can be observed from the lower absolute reverse stream axial velocity at the fan outlet plane for the N_2 speed from hub to 80% span. The amount of reverse stream that escapes out at the fan inlet plane is also consequently lower than the higher rotational

speed case as evidenced by the flow feature '1' and the lower axial velocity near the casing at fan inlet plane. In the lower speed case, the radial migration of both the streams within the passages proceeds to a higher radial extent before the reverse stream turns back onto itself in the fan outlet plane because of the lower momentum of the reverse stream. This is observed in the higher span wise extent at which reverse flow is turned back to the nozzle exit in the fan outlet plane for the N_2 speed.

The installed bi-directional flow field change with rotational speed is required to choose the fan rotational speed for operation in reverse thrust during the landing run. While the VPF only clean reverse flow characteristics may capture the reduction in the reverse flow stream momentum, the consequences of such reduced momentum on the interaction with the free stream and the flow direction change can only be captured using an installed model as in this study.

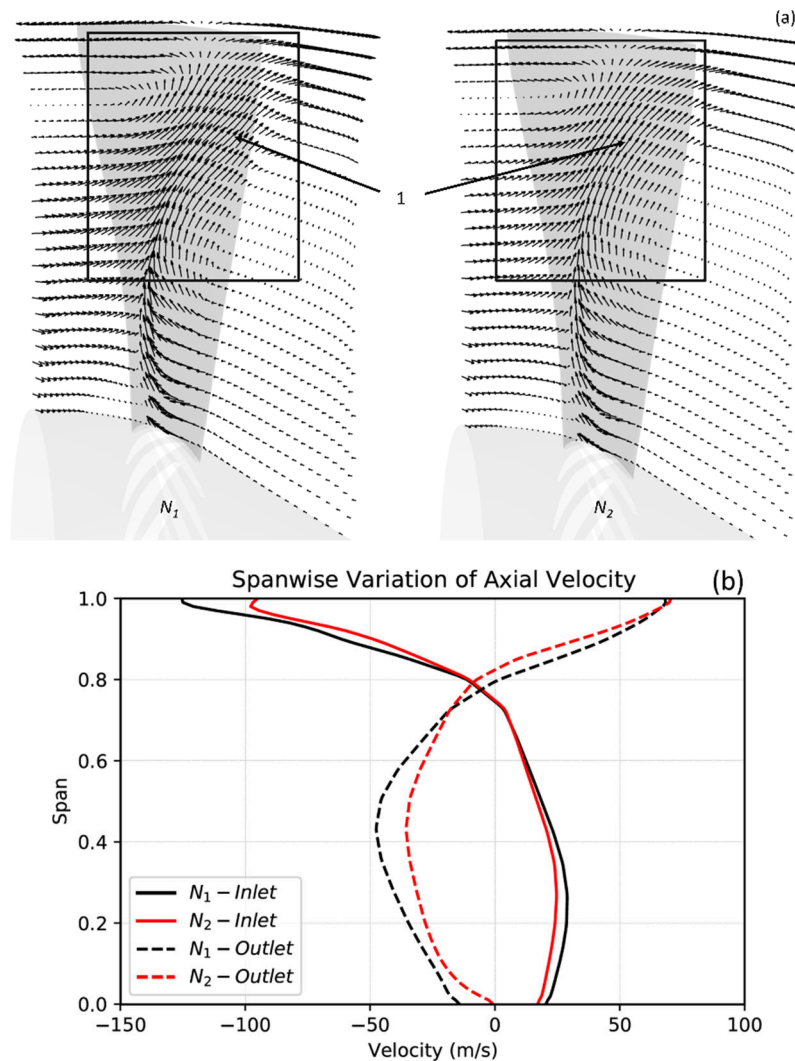


Fig. 13 Effect of fan speed change – (a) Meridional velocity vectors (b) Span-wise averaged axial velocity plot

Effect of Aircraft Landing Speed on Fan Flow Field

The change in the fan flow field for the VPF at ζ_l° stagger angle setting and N_l rotational speed with the change in the aircraft landing speed is described in this section by considering three representative landing speeds, 140, 80 and 20 knots. These speeds represent the beginning, middle and end of a typical aircraft landing run. It is to be noted that in general reverse thrust systems are disengaged at a landing speed of around 50 knots to prevent foreign object ingestion. However, in this discussion the 20 knots case is considered to clearly elucidate the extent of change in the fan flow field. A comparison of the circumferentially averaged meridional absolute velocity vector plots and span-wise variation of axial velocities for the different landing speeds are shown in Fig. 14.

As the landing speed of the aircraft decreases, the following changes can be observed: 1. the amount of reverse flow entering the bypass nozzle exit increases because of the fan suction acting on slower moving air at the engine exit. This increase can be observed in the increase in absolute reverse stream axial velocity at the fan outlet plane from hub to 80% span. 2. The free stream momentum decreases as can be observed from the axial velocity at the fan inlet plane from hub to the span of reverse flow turnover 3. The increase in the reverse flow momentum and the reduction in the free stream momentum leads to an increase in the amount and momentum of the flow escaping near the casing at the fan inlet plane as seen in the larger regions bound between the reverse stream marker and the casing in the vector plots. This causes an increase of the span-wise portion which the reverse stream occupies at the fan inlet plane from 20% of span at 140 knots to 40% of span at 20 knots as observed from the axial velocities in the fan inlet plane. 4. There is an increase in the chord-wise location with respect to the fan outlet plane from which the reverse flow at the fan outlet plane turns back. This is a consequence of the higher momentum of the reverse flow that changes the direction of the radial migration of both the streams. The signature of this deeper penetration before reversal can be seen as a kink in the axial velocity distribution at 20 knots in the fan inlet plane near the casing from 80% span to the casing.

This change in the flow field with landing speed that cannot be obtained from an uninstalled reverse flow only model is essential to choose the appropriate VPF operational setting in terms of stagger angle and rotational speed to deliver the required reverse thrust during the entire landing run.

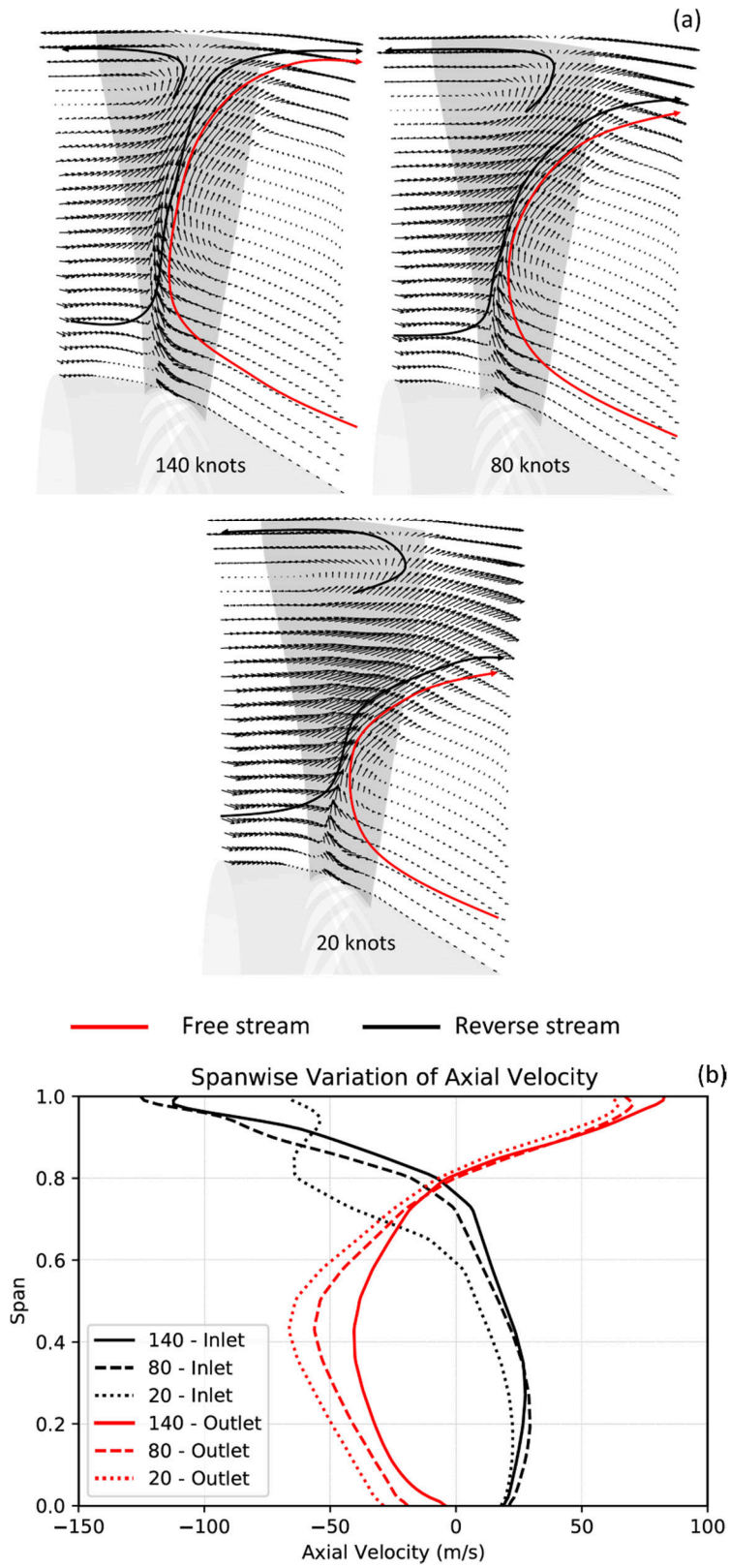


Fig. 14 Effect of aircraft landing speed change – (a) Meridional velocity vectors (b) Span-wise averaged axial velocity plot

CONCLUSIONS

A newly developed integrated airframe-engine model is used to describe the installed fan flow field in two representative reverse thrust VPF stagger angle settings, ζ_1° and ζ_2° , and two fan rotational speeds, N_1 and N_2 . This study has resulted in:

1. Complete description of flow features external and internal to the engine that determine the actual flow conditions that the VPF design will need to operate in installed conditions. This is different from the typical uninstalled reverse flow only analyses that are used in the VPF design process.
2. Identification of a bi-directional flow at the fan inlet and outlet planes because of the interaction between the reverse flow and the free stream flow. Conventional design processes consider only the reverse stream. The fan behavior in terms of mass flow and pressure ratio for the installed bi-directional flow field is different from the uninstalled VPF only clean reverse flow characteristics. Therefore, only the installed flow field can provide realistic estimates of the actual amount and momentum of reverse flow that can contribute to reverse thrust.
3. Description of the change in fan flow field with stagger angle setting, rotational speed and landing speed that is required to choose the operating setting of the VPF during the aircraft landing run to generate the required reverse thrust.
4. The change in the installed fan flow field description with landing speed indicates the broad range of operating conditions that the VPF design needs to operate in. The bi-directional flow of the installed model changes the fan blade loading as compared to the traditional reverse flow only static solutions used in the VPF design process. Therefore, any blade profile modifications carried out in the design process need to be verified for its operability in an actual installed flow field.
5. Availability of a vehicle research model that can form the apex of the VPF design process to verify and qualify different designs in actual installed conditions. The same model can be used to test design changes in different parts of the engine and aircraft geometry that can contribute to improving the levels of reverse thrust.

It is realized from the study that the VPF flow field in reverse thrust may have temporal variations because of the interaction of the reverse stream and the free stream. An unsteady analysis is currently underway to provide further insights into the temporal installed fan flow field development. A methodology to characterize any installed VPF design in the novel bi-directional flow field to generate ready look-up tables to describe the fan operating point and

the corresponding levels of reverse thrust produced is planned. Finally, it is envisioned to validate the description of the installed flow field obtained from the 3D RANS solution by using an aerodynamic test rig in which a scaled installed reverse flow VPF design is operated at different free stream velocities.

ACKNOWLEDGMENT

The authors would like to express their gratitude to Rolls-Royce plc. for supporting this research and for permission to publish the paper. Special thanks to Mr. Richard Tunstall, Mr. John Whurr and Mr. David Foster of Rolls-Royce plc. for comments and suggestions.

NOMENCLATURE

Abbreviations

ADP	Advanced Ducted Propulsor
CRM	Common Research Model
GCI	Grid Convergence Index
OGV	Outlet Guide Vane
QCSEE	Quiet Clean Short-haul Experimental Engine
RANS	Reynolds-Averaged Navier Stokes
VPF	Variable Pitch Fan

Symbols

N	Fan rotational speed
r_h	Hub radius
r_t	Tip radius
ζ	Stagger angle

REFERENCES

[1] Mazzawy, R.S., 2010, "Performance Study for the Benefits of a Variable Pitch Composite Fan," In ASME Turbo Expo 2010: Power for Land, Sea, and Air (pp. 37-45). American Society of Mechanical Engineers.

- [2] Krishnan, G., Perullo, C. and Mavris, D.N., 2013, "An Assessment of Relative Technology Benefits of a Variable Pitch Fan and Variable Area Nozzle," In 49th AIAA/ASME/SAE/ASEE Joint Propulsion Conference (p. 3604), DOI: 10.2514/6.2013-3604
- [3] Denning, R.M., 1972, "Variable Pitch Ducted Fans for STOL Transport Aircraft," In ASME 1972 International Gas Turbine and Fluids Engineering Conference and Products Show (pp. V001T01A060-V001T01A060), American Society of Mechanical Engineers. ISBN: 978-0-7918-7981-8, DOI: 10.1115/72-GT-61
- [4] Halliwell, I. and Justice, K., 2012, "Fuel Burn Benefits of a Variable-Pitch Geared Fan Engine," In 48th AIAA/ASME/SAE/ASEE Joint Propulsion Conference & Exhibit (p. 3912), DOI: 10.2514/6.2012-3912
- [5] Violette, J.A. and Loos, E.S., 2010, "Mechanical Design of a Variable Pitch Fan for Turbofan Engines." In ASME Turbo Expo 2010: Power for Land, Sea, and Air (pp. 303-308), American Society of Mechanical Engineers, ISBN: 978-0-7918-4396-3, eISBN: 978-0-7918-3872-3, DOI: 10.1115/GT2010-22969
- [6] McKay, B. and Barlow, A., 2012, "The UltraFan Engine and Aircraft Based Thrust Reversing," In 48th AIAA/ASME/SAE/ASEE Joint Propulsion Conference & Exhibit (p. 3919). DOI: 10.2514/6.2012-3919
- [7] Moore, R.D. and Osborn, W.M., 1979, "Aerodynamic performance of 1.38-pressure-ratio, variable-pitch fan stage," NASA Technical Paper, NASA TP 1502. NASA Scientific and Technical Information Branch, Document ID: 19790023042, Accession Number: 79N31213.
- [8] Moore, R.D. and Kovich, G., 1976, "Aerodynamic performance of two variable-pitch fan stages," NASA Technical Memorandum, NASA TM X-73416. NASA Scientific and Technical Information Branch, Document ID: 19760019066, Accession Number: 76N26154.
- [9] Samanich, N.E., Reemsnyder, D.C. and Bloomer, H.E., 1980, "Reverse thrust performance of the QCSEE variable pitch turbofan engine," SAE Transactions, Vol. 89, Section 4: 801147–801431 (1980), pp.3623-3650, <http://www.jstor.org/stable/44632622>
- [10] Schaefer, J.W., Sagerser, D.R. and Stakolich, E.G., 1977, "Dynamics of high-bypass-engine thrust reversal using a variable-pitch fan," NASA Technical Memorandum, NASA TM X-3524. NASA Scientific and Technical Information Branch, Document ID: 19770015162, Accession Number: 77N22106.
- [11] Reemsnyder, D.C. and Sagerser, D.A., 1979, "Reverse Thrust Performance of a Variable-Pitch Fan Engine at Forward Velocity," Journal of Aircraft, 16(12), pp.848-855. DOI: 10.2514/3.58612

- [12] Jeracki, R.J., 2006, "Comprehensive report of fan performance from duct rake instrumentation on 1.294 pressure ratio, 806 ft/sec tip speed turbofan simulator models," NASA Technical Memorandum, NASA/TM-2006-213863. NASA Scientific and Technical Information Branch, Document ID: 20060007570.
- [13] Hobbs, D.E., Neubert, R.J., Malmborg, E.W., Philbrick, D.H. and Spear, D.A., 1995, "Low Noise Research Fan Stage Design," NASA Contractor Report, NASA-CR-195382. Prepared under contract NAS3-26618. NASA Scientific and Technical Information Branch, Document ID: 19990095609.
- [14] Tweedt, D.L., 2014, "Computational aerodynamic simulations of an 840 ft/sec tip speed advanced ducted propulsor fan system model for acoustic methods assessment and development," NASA Contractor Report, NASA/CR-2014-218129. Prepared under contract NNC06BA07B. NASA Scientific and Technical Information Branch, Document ID: 20140016376.
- [15] Williams, TS. and Hall, CA., 2018, "Reverse Thrust Aerodynamics of Variable Pitch Fans," ASME. Turbo Expo: Power for Land, Sea, and Air, Volume 2A: Turbomachinery ():V02AT39A014. DOI: 10.1115/GT2018-75739
- [16] Palmer, J.R. and Pachidis, V., 1990, "The TURBOMATCH scheme for aero/industrial gas turbine engine design point/off design performance calculation," SME, Thermal Power Group, Cranfield University.
- [17] Mourouzidis, C., 2016, "Cycle Optimisation & Preliminary Design of Very Low Specific Thrust Turbofan Engines," Ph.D thesis, School of Aerospace, Transport & Manufacturing, Cranfield University.
- [18] Lolis, P., 2014, "Development of a preliminary weight estimation method for advanced turbofan engines," Ph.D thesis, School of Aerospace, Transport & Manufacturing, Cranfield University, <http://dspace.lib.cranfield.ac.uk/handle/1826/9244>.
- [19] Lolis, P., Giannakakis, P., Sethi, V., Jackson, A.J.B. and Pilidis, P., 2014, "Evaluation of aero gas turbine preliminary weight estimation methods," The Aeronautical Journal, 118(1204), pp.625-641.
- [20] Templalexis, I., Pilidis, P., Pachidis, V. and Kotsiopoulos, P., 2006, "Quasi-three-dimensional compressor performance simulation using streamline curvature and multi-parallel compressor theory," In ASME Turbo Expo 2006: Power for Land, Sea, and Air (pp. 297-309). American Society of Mechanical Engineers, ISBN: 0-7918-4239-8, DOI: 10.1115/GT2006-90812
- [21] Rumsey, C.L. and Slotnick, J.P., 2014, "Overview and summary of the second AIAA High Lift Prediction Workshop," In 52nd Aerospace Sciences Meeting (p. 0747), DOI: 10.2514/6.2014-0747

- [22] AIAA, 2013, The 2nd AIAA CFD High Lift Prediction Workshop (HiLiftPW-2). [online] LARC NASA. Available at: <https://hiliftpw.larc.nasa.gov/index-workshop2.html> [Accessed 15 March 2018].
- [23] Blasco, D.C., 2017, "3D-CFD Model Design and Intergration of a Variable Pitch Fan Engine," M.Sc thesis, School of Aerospace, Transport & Manufacturing, Cranfield University.
- [24] Goulos, I., Giangaspero, G., MacManus, D., 2017, "GEMINI v2.0 User-Guide," Rolls Royce UTC in Performance Document.
- [25] Stankowski, T.P., MacManus, D.G., Sheaf, C.T. and Grech, N., 2016, "Aerodynamic interference for aero-engine installations," In 54th AIAA Aerospace Sciences Meeting (p. 0766), DOI: 10.2514/6.2016-0766

APPENDIX A – 'VPF TO GENERATE REVERSE THRUST'

VPF can be used to generate reverse thrust by changing the direction of the fan airflow. This can be achieved by rotating the stagger angle of the fan blades by 90° in either the clockwise or anti-clockwise direction. The rotation in the clockwise direction, typically called 'through-flat pitch', may be constrained by the pitch-chord ratio of the fan blades. The anti-clockwise rotation is called 'through-feather pitch' because the rotation takes place through an axially feathered fan blade setting as in propellers. The 'through-feather pitch' is better suited because it does not place any restrictions on the nominal fan design pitch-chord ratio. When the fan blades are rotated through feather pitch, the capture throat area of the fan cascade shifts from leading edge (blackened) to the trailing edge of the cascade, causing airflow to be sucked in from behind the cascade as shown in Fig.A1 [7].

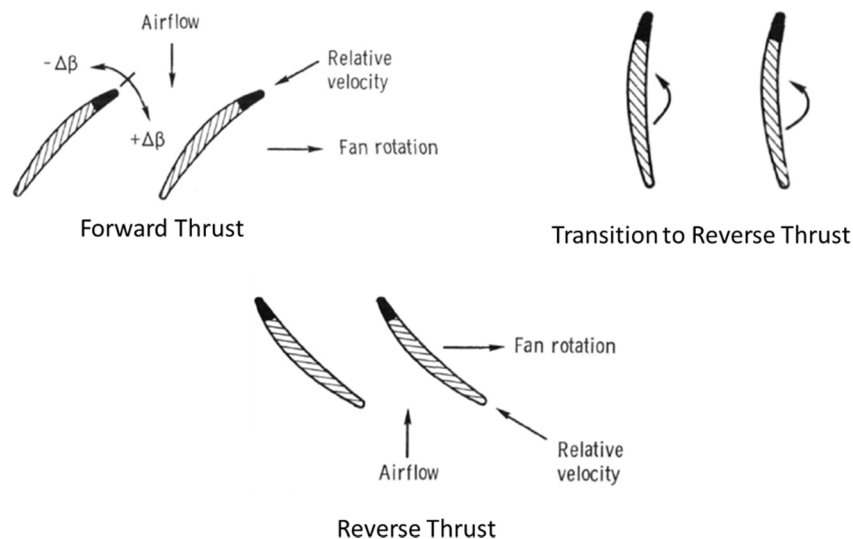


Fig. A1 Schematic showing change in airflow direction with change in stagger angle

Fan flow field in an installed variable pitch fan operating in reverse thrust for a range of aircraft landing speeds

Rajendran, David John

2019-09-20

Attribution 4.0 International

Rajendran DJ, Pachidis V. (2019) Fan flow field in an installed variable pitch fan operating in reverse thrust for a range of aircraft landing speeds. *Journal of Engineering for Gas Turbines and Power*, Volume 141, Issue 10, October 2019, Article number 101018

<https://doi.org/10.1115/1.4044686>

Downloaded from CERES Research Repository, Cranfield University